ELSEVIER J. Non-Newtonian Fluid Mech., 59 (1995) 129–153

Journal of Non-Newtonian Fluid Mechanics

The experimental observation and numerical prediction of planar entry flow and die swell for molten polyethylenes

R. Ahmed, R.F. Liang[1], M.R. Mackley*

Department of Chemical Engineering, University of Cambridge, Pembroke Street, Cambridge CB2 3RA, UK

Received 10 October 1994; in revised form 13 February 1995

Abstract

We report experimental observations and matching numerical simulations for the planar entry flow and die swell of two high-density polyethylenes (HDPEs) and one low-density polyethylene (LDPE). Experimental data for stress fields, centreline velocities and die swell are reported for each polymer. These results are compared with numerical simulation. The materials are characterized in simple shear using a Wagner integral constitutive equation with a discrete spectrum of relaxation times and a single parameter damping function. The numerical simulation has been carried out using a finite element software package, Polyflow. Self consistency in the stress and die swell data are found for one HDPE, but the other HDPE and the LDPE show an extensional strain hardening response which is not predicted using the simple shear rheology data. In the latter cases, the numerical predictions consistent with entry flow experimental observations can be achieved if extensional flow damping parameters, rather than simple shear damping parameters, are chosen. For the LDPE, an increase in the strain hardening parameter results in the numerical prediction of upstream recirculation vortices in the entry region, which qualitatively agrees with the experimental observations. Apparent inconsistencies in the absolute values of measured and simulated velocity profiles are explained in terms of the 2D nature of the simulation and a 3D component to the experimental flow.

Keywords: Die swell; Experimental observation; Planar entry flow; Polyethylene melt; Numerical simulation; Wagner integral equation.

* Corresponding author.

[1] Permanent address: Institute of Chemistry, Academia Sinica, Beijing 100080, China.

SSDI 0377-0257(95)01358-X

1. Introduction

This paper is concerned with the comparison of experimental data and numerical simulation in relation to the way in which molten polyethylene flows into and out of a contraction. In particular, it is concerned with the extensional flow behaviour of polyethylene in an entry flow and the ability to simulate this behaviour using simple shear rheological data.

The entry and exit flow behaviour is of central importance to the understanding of many aspects of polymer processing, and the subject has been reviewed by Ahmed and Mackley [1] whose work forms the starting point of this study. In that paper, simple shear rheometric data were fitted to a Wagner integral constitutive equation using a discrete spectrum of relaxation times and a single parameter exponential damping function. Using experimentally determined centreline velocity profiles, the predictions of the constitutive equation were compared with the centreline stress distributions obtained experimentally using flow birefringence techniques for two molten polyethylenes flowing into a slit. The results showed that self consistency was found for one polymer HDPE "Natene". However, for the other polymer HDPE "Rigidex", there was an inconsistency between the constitutive equation prediction and the observed results.

In this paper, we cover both entry and exit flows for three molten polyethylenes and concentrate our attention on the importance of the correct extensional flow description of the materials under investigation. In addition, we introduce a global numerical simulation of the problem. Rheological characterization in simple shear is carried out using a previously described method (Ahmed and Mackley [1]). Experimental stress and velocity fields are also obtained in the same way as described by Ahmed and Mackley [1], Aldhouse et al. [2], and Mackley and Moore [3]. The experimental centreline and global stress distributions, velocity distributions, die swell data and vortex recirculation are then compared with numerical simulations using Polyflow.

Recent development in numerical computation of, in particular, integral type viscoelastic constitutive equations has enabled simulated predictions of both the entry and exit flow of polymer melts (see, for example, Crochet and Walters [4], Dupont and Crochet [5], van Gurp et al. [6], and Feigl and Ottinger [7]). Park et al. [8] and Kiriakidis et al. [9] have predicted the stress distribution and the extrudate swell, and compared stress fields with experimental data for a high-density polyethylene and a linear low-density polyethylene respectively. Goublomme and co-workers [10,11] have simulated the extrudate swell for a high-density polyethylene and compared their simulations with experimental results (see Koopmans [12]).

In the last few years, Polyflow has been developed into a sophisticated numerical package for steady polymer flow [4,13,14]. In the present work, we use it to model the molten polymer flow through a slit with similar boundary conditions to the experiments. In the first instance, we use the Wagner integral constitutive equation with parameters derived from simple shear rheometric data. In order to obtain improved matching for entry flow, the damping function parameter in some cases

is subsequently adjusted. Both experimental data and numerical simulations will show just how sensitive the polymer extrusion process can be to rheological differences in the flowing material and, in particular, how the entry flow rheology of molten polymers can have a significant effect on the ultimate processability of the materials.

2. Constitutive equation

The constitutive equation used is a K-BKZ equation of the separable type, as proposed by Wagner [15], and can be expressed in its general form as follows:

$$\tau(t) = -\int_{-\infty}^{t} \sum_i \frac{g_i}{\lambda_i} e^{-(t-t')/\lambda_i} h(I_1,I_2)\mathbf{C}^{-1}(t,t')\,dt', \tag{1}$$

where $\tau(t)$ is the stress tensor at time t, (g_i,λ_i) are the discrete spectrum of relaxation modulus and relaxation time respectively, $\mathbf{C}^{-1}(t,t')$ is the Finger strain tensor which describes the deformation of a fluid element between the present time t and past time t', and $h(I_1,I_2)$ is the damping function which is assumed to be of an exponential form (see Wagner [16]):

$$h(I_1,I_2) = e^{-k[\beta I_1 + (1-\beta)I_2 - 3]^{0.5}}, \tag{2}$$

where I_1 and I_2 are the first and second invariants of the Finger tensor, k is the damping coefficient which is determined in simple shear and β is the damping coefficient which is introduced for extensional flow (see also Dealy and Wissbrun [17]).

In simple shear, we have

$$I_1 = I_2 = \gamma^2(t,t') + 3, \tag{3}$$

where γ is the shear strain. The β parameter in Eq. (2) becomes irrelevant. From Eq. (1), the shear stress $\tau_{12}(t)$ is given in terms of the past strain deformation $\gamma(t,t')$ by

$$\tau_{12}(t) = -\int_{-\infty}^{t} \sum_i \frac{g_i}{\lambda_i} e^{-(t-t')/\lambda_i} e^{-k|\gamma(t,t')|}\gamma(t,t')\,dt', \tag{4}$$

Therefore, the rheological response in simple shear is fully modelled using the Wagner integral constitutive equation with a discrete spectrum of relaxation times and a single parameter damping function.

In planar extensional flow, the Finger strain tensor yields

$$I_1 = I_2 = \lambda^2(t,t') + \lambda^{-2}(t,t') + 1, \tag{5}$$

where λ is the stretching ratio. The β parameter in Eq. (2) also does not enter Eq. (1). The extensional stress $[\tau_{11}(t) - \tau_{22}(t)]$ is given in terms of the stretch ratio $\lambda(t,t')$ by

$$\tau_{11}(t) - \tau_{22}(t) = -\int_{-\infty}^{t} \sum_i \frac{g_i}{\lambda_i} e^{-(t-t')/\lambda_i} e^{-k[\lambda^2(t,t') + \lambda^{-2}(t,t') - 2]^{0.5}} \times [\lambda^2(t,t') - \lambda^{-2}(t,t')]\, dt' \quad (6)$$

According to Eq. (6), the extensional stress can also be described using the model with the relaxation spectrum and the damping function coefficient which is determined in simple shear.

Eq. (4) was found to be very successful in describing rheological behaviour in simple shear for, in particular, polymer melts and solutions and a number of other fluids in general (see, for example, Laun [18], and recent work by Mackley et al. [19], and Liang and Mackley [20]). We therefore have confidence in the ability of the chosen constitutive equation, at least to characterize simple shear response.

The present work will check the validity of Eq. (6) in describing a 2D planar extensional flow of the material using simple shear parameters. For this purpose, we obtain relaxation spectra (g_i,λ_i) from the dynamic storage and loss moduli by means of Rheometrics software. We determine the damping function coefficient from linear and non-linear step-strain experimental results. The strain history of the material is calculated from the flow kinematics, which is generated either numerically by the simulation software, Polyflow, itself, or experimentally using the laser velocimetry technique. The self consistency of the material between simple shear and extension can be identified from a comparison between the predicted and measured stress data.

The die swell behaviour of the polymer melt can also be predicted in terms of Eq. (6) by the use of Polyflow. For the computation of the die swell, we need to further specify whether an irreversibility assumption of the damping function applies or not. The irreversibility assumption suggested by Wagner and Stephenson [21] states that the damping function only decreases irreversibly (see also Goublomme et al. [10], and Dealy and Wissbrun [17]). In our experiment, the flow of the polymer melt emerging from the slit exit and into a free surface cavity to swell produces a reversing deformation. No irreversibility assumption would allow the damping function to increase again. In the present study, we have checked the irreversibility assumption; it has no effect on the entry flow, but can influence the die swell response. In this paper, unless stated otherwise, all the simulation results are obtained using an irreversible Wagner damping function.

3. Materials and simple shear characterization

The materials tested include two high-density polyethylenes (HDPEs), Natene and Rigidex, and one low-density polyethylene (LDPE). HDPE Natene and Rigidex were known to have the same melt flow index (MFI), similar flow curves, but different die swell behaviour. A branched LDPE was also chosen, as this material showed a striking difference in the entry flow behaviour. Some properties of the materials are given in Table 1. These three BP grade polyethylenes form

Table 1
Some properties of three polyethylenes tested

Polymer	Density ($kg\ m^{-3}$)	MFI g $(10\ min)^{-1}$	$M_w \times 10^5$	$M_n \times 10^4$	M_w/M_n
Natene	952	10	3.1	0.8	39
Rigidex	952	10	2.4	2.0	12
LDPE	921	0.3	–	–	–

M_w; weight average molecular mass; M_n; number average molecular mass.

representative examples of a larger set that have been examined in simple shear and extensional flow.

Simple shear measurements were made on a Rheometrics RDSII Mechanical Spectrometer with parallel plates with a diameter of 25 mm and a gap of 1 mm at 180°C. The material parameters for Eq. (6) are determined using a standard procedure as follows. The discrete relaxation spectrum, (g_i,λ_i) are obtained from the linear viscoelastic oscillatory data, $G'(\omega)$ and $G''(\omega)$ by use of on-line Rheometrics software. The data were collected over the frequency range 0.001–100 rad s^{-1}. Eight time constants are used for the present study. The damping function coefficient k is calculated from the linear and non-linear step-strain relaxation moduli, and the details of the method are given by Ahmed and Mackley [1]. Table 2 gives data for the relaxation spectrum and damping function coefficient for three polyethylene melts at 180°C. Using these parameters and Eq. (4), good self consistency in simple shear between the experiment and the prediction for each polymer has been checked as reported by Ahmed and Mackley [1].

Table 2
Simple shear (g_i, λ_i) and k for three polyethylene melts (at 180°C)

Natene $k = 0.30 \pm 0.05$		Rigidex $k = 0.37 \pm 0.05$		LDPE $k = 0.16 \pm 0.02$	
λ_i (s)	g_i (Pa)	λ_i (s)	g_i (Pa)	λ_i (s)	g_i (Pa)
0.002	211910	0.001	303600	0.002	124030
0.00938	76242	0.00518	140700	0.00746	24607
0.044	64017	0.0268	100100	0.0278	35360
0.2065	34310	0.1389	47000	0.1036	19265
0.9686	18545	0.7197	21400	0.3861	12558
4.544	9842.1	3.728	7667	1.4394	7297.6
21.32	3845.2	19.31	2764	5.3654	2709.5
100.0	2042.6	100.0	1448	20.0	1632.6

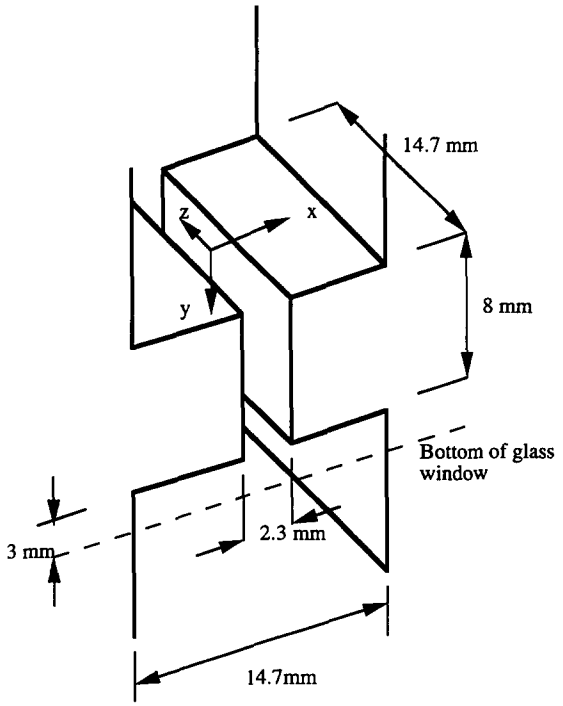

Fig. 1. A schematic diagram of the slit die and the configuration of the window where x is the width direction, y is the flow direction and z is the depth direction.

4. Experimental techniques on molten polymer flows through a slit

The polymer melt flows first through an extruder barrel, then a melt pump followed by a connection arm, and finally into and out of a flow cell which is maintained at a temperature of 180°C (see Ahmed and Mackley [1]). An abrupt entry slit die is confined between two glass windows within the flow cell and, as a result, a near planar extensional flow of molten polymer takes place along the centreline. After flowing out of the slit, the polymer melt emerges into a free surface cavity and the swell of the extrudate occurs. Mass flow rates of 0.22, 0.32 and 0.44 g s^{-1} were considered. A schematic diagram of the slit die and the configuration of the window is shown in Fig. 1. The slit has a length of 8 mm, a width of 2.3 mm and a depth of 14.7 mm. The entry upstream has a length of 14.7 mm, a width of 14.7 mm and a depth of 14.7 mm. Thus, the contraction ratio of the studied entry flow is 6.39:1.

Experimental measurements on molten polymer flows through the slit included flow birefringence observation and laser Doppler velocimetry over the flow field through the flow cell. From the flow birefringence pattern, we are able to determine the global stress field in general and the centreline stress profile in particular using the stress optical law:

$$n_{11} - n_{22} = C(\sigma_{11} - \sigma_{22}), \tag{7}$$

where $n_{11} - n_{22}$ is the principal birefringence index, $\sigma_{11} - \sigma_{22}$ is the principal stress difference (PSD) and C is the stress optical coefficient. The stress optical coefficient used in this work is 1.84×10^{-9} m^2 N^{-1} for HDPE at 180°C and 1.87×10^{-9} m^2 N^{-1} for LDPE at 18O°C (see Ahmed and Mackley [1]). The laser velocimetry technique enables us to obtain information on the flow kinematics. The deformation history is calculated from the centreline velocity profile and used for the prediction of the centreline stress from Eq. (6). Details of the experimental techniques can be found in the previous paper [1]. The die swell behaviour of the extrudate was also determined using a video-image method and data are presented as the initial die swell ratio, which was the swelling ratio of the emerging polymer melt 2 mm downstream from the slit exit and at the extrusion temperature 180°C.

5. Numerical approach

The aim of our numerical simulation is to model the molten polymer flow using the experimental slit boundary conditions and compare the simulation with the experimental observation, in order to check the applicability of the chosen constitutive equation and constitutive parameters.

Numerical simulations were carried out using Polyflow software. Polyflow is a commercial finite element package developed by Professor Crochet and his team [4,13,14]. The Polyflow version we used is Polyflow (3.2.0). The procedures for solving a general viscoelastic flow problem can be summarized as follows. Firstly, using a Polymesh program, a mesh in terms of the flow geometry is generated. Secondly, using the Polydata program, the mesh file is combined with the constitutive equation, material parameters and boundary conditions. This is then used as an input to run the Polyflow program. Finally, using a post-processing program, Polyplot, the results can be visualized.

The finite element numerical technique used by Polyflow involves solving the field equations initially for a Newtonian fluid. An evolution parameter is then introduced which progressively transfers the Newtonian constitutive equation to that of the chosen viscoelastic form. At each stage of the evolution, a convergence criterion is applied, and using this method it is possible to obtain stable time-independent solutions for all of the parameters and boundary conditions reported in this paper. Details of the numerical algorithm can be found in Refs. [5], [10], [11], [13] and [14].

The numerical computations described in this paper took typically three days for each calculation using a dedicated Sun workstation. These long computation times restricted us to the simulations of two-dimensional flow. The laboratory experiments were dominantly two dimensional, but did have a weak third-dimensional velocity component.

Four finite element meshes have been designed for the computation at different stages. These meshes are shown in Fig. 2, and their geometry sizes are defined in Table 3 in comparison with the geometry size of the experimental slit. The number

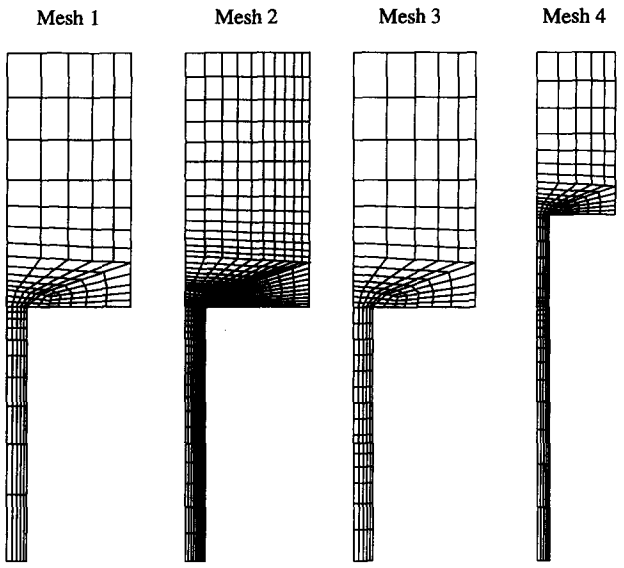

Fig. 2. The finite element meshes used in the computation for the planar entry flow (Mesh 1 and Mesh 2) and the free surface (Mesh 3 and Mesh 4). The geometry sizes are defined in Table 3.

of finite elements is also listed for each mesh. Mesh 2 is a refined version of Mesh 1 and has four times the number of elements in Mesh 1. Mesh 1 and Mesh 2 were used in the entry flow simulation for HDPE Natene and Rigidex before we took the exit flow into consideration. It was found that the refinement of the mesh had no effect on the predictions. Mesh 3 and Mesh 4 were used for the free surface simulation. The difference between Mesh 3 and Mesh 4 is that Mesh 4 has a longer free surface downstream. The data reported here are based on Mesh 4 for Natene and Rigidex, and Mesh 2 for LDPE.

Table 3
Experimental slit geometry and 2D mesh size

	Exp. slit	Mesh 1	Mesh 2	Mesh 3	Mesh 4
Length (mm)					
upstream	14.7	15	15	15	15
downstream	8	15	15	7.5	8
free-surface	–	–	–	7.5	24
Width (mm)					
upstream	14.7	14.7	14.7	14.7	14.7
downstream	2.3	2.3	2.3	2.3	2.3
Depth (mm)	14.7	(14.7)	(14.7)	(14.7)	(14.7)
No. of elem.	–	156	624	181	221

The boundary conditions we applied are as follows: for Mesh 1 and Mesh 2, a fully developed flow ($v_s = 0$, flow rate Q) as inflow, no slip ($v_s = 0$, $v_n = 0$) at the wall, a fully developed flow ($v_s = 0$, flow rate Q) as outflow and planar symmetry ($f_s = 0$, $v_n = 0$); for Mesh 3 and Mesh 4, a fully developed flow ($v_s = 0$, flow rate Q) as inflow, no slip ($v_s = 0$, $v_n = 0$) at the wall, free surface after the slit exit, ($f_n = 0$, $f_s = 0$) as outlet and planar symmetry ($f_s = 0$, $v_n = 0$). Here, v is the velocity, f is the force, subscript s stands for tangential direction and subscript n stands for normal direction.

In Polyflow, the stress tensor is calculated by defining a post-processor sub-task and the stress component τ_{ij} is obtained. In order to carry out a comparison with the experimental stress data obtained from flow birefringence, the principal stress σ_{ii} and PSD are calculated using the following equations:

$$\sigma_{11} = \frac{\tau_{11} + \tau_{22}}{2} + \left[\left(\frac{\tau_{11} - \tau_{22}}{2}\right)^2 + \tau_{12}^2\right]^{1/2}, \tag{8}$$

$$\sigma_{11} = \frac{\tau_{11} + \tau_{22}}{2} - \left[\left(\frac{\tau_{11} - \tau_{22}}{2}\right)^2 + \tau_{12}^2\right]^{1/2}, \tag{9}$$

$$\mathrm{PSD} = \sigma_{11} - \sigma_{22} = 2\left[\left(\frac{\tau_{11} - \tau_{22}}{2}\right)^2 + \tau_{12}^2\right]^{1/2}. \tag{10}$$

Along the centreline, the shear stress component τ_{12} is zero and the PSD is defined as extensional stress. In the graphs of numerical PSD contours, the same stress increment, 1.9249×10^4 Pa for HDPE and 1.9898×10^4 Pa for LDPE, as in the flow birefringence pattern, has been used for direct comparison.

In addition to the simulation using Polyflow, the centreline stress profile is also predicted using Eq. (6) incorporated with the relaxation spectrum, a damping function coefficient and the experimentally measured flow kinematics. These results are then compared with those obtained using Polyflow.

6. Results

6.1. The flow behaviour of HDPE "Natene"

The simulated and experimental responses of HDPE Natene are shown in Figs. 3–6. The simulated streamlines for the material are given in Fig. 3, and show a typical entry and die swell profile which is consistent with experimental observations. This HDPE did not experimentally exhibit upstream recirculation, and with a damping parameter $k = 0.35$ the simulation did not predict them either.

The experimental principal stress contours for Natene at a flow rate of 0.22 g s^{-1} and a temperature of 180°C are shown in Fig. 4(a), and can be directly compared with the simulated response given in Fig. 4(b). The overall matching of contours and die swell profile is considered to be good. The predicted stress fields upstream, within the die and in the exit region, all show semi-quantitative agreement with the experimental results. The weakest area of prediction appears to be the centreline,

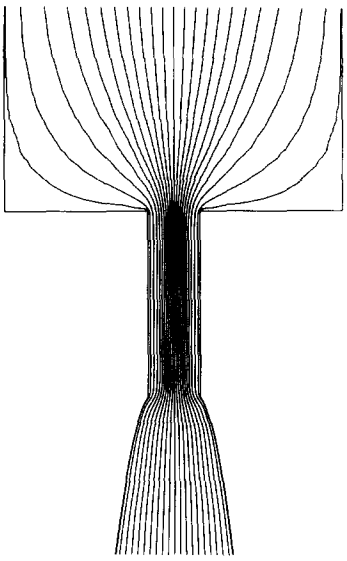

Fig. 3. Simulated streamline pattern for HDPE Natene flowing into, within and out of the slit at a flow rate of 0.22 g s^{-1} and temperature of 180°C (Mesh 4, $k = 0.35$).

far-upstream simulated contour, which predicts a heart shape contour that is not seen experimentally.

Figs. 5(a) and 5(b) show simulated and experimental data for a higher flow rate of 0.32 g s^{-1}, and again overall agreement is good with the exception of the simulated upstream heart shape.

A quantitative comparison in the stress profile between experiment and prediction was made along the centreline of the geometry. The centreline stress profiles are shown in Fig. 6 for Natene flowing through the slit at 0.32 g s^{-1} and 180°C. The PSD is plotted as a function of axial position starting from the entry upstream with the slit entrance at O.O15 m and the slit exit at 0.023 m. As seen from Fig. 6, a good fit with the experimental data is obtained from the numerical simulation using Polyflow with a k value of 0.35. Fig. 6 also includes the centreline stress distribution predicted by following the experimental flow kinematics using laser velocimetry and using our own program for the centreline prediction (see Ahmed and Mackley [1]). In the centreline prediction, the non-linear damping function coefficient was 0.30. It is seen that both numerical approaches are able to provide correct predictions, not only for the entry convergent flow but also for the exit flow. Fig. 6 clearly shows the stress build-up and decay process when the polymer melt flows into, within and out of the slit die. The only region of significant deviation in Fig. 6 between the three plots is in the centreline relaxation within the slit using our own experimental velocity field data. We are now suspicious that the fluctuations in laser velocimeter data within the slit gave rise to this apparent inconsistency. The matching of the peak stresses in the throat of slit together with the stress decay in the die swell region both appear to give impressive agreement.

This total set of data for HDPE Natene is important in that it shows both global and centreline self consistency. Using rheological parameters obtained in simple shear we have been able to successfully predict flow contours and stress fields for this material in an entry and exit flow.

6.2. *The stress field for HDPE "Rigidex"*

The flow behaviour of HDPE Rigidex is shown in Figs. 7 and 8. The experimental stress contours are shown in Fig. 7(a) for a flow rate of 0.22 g s^{-1} and at 180°C. These contours make an interesting comparison with those of HDPE Natene shown in Fig. 4(a). Qualitatively, the upstream contours are similar; however, within the slit, the shapes of the contours in the throat region have a different form. Neither HDPE has recirculating upstream vortices.

Fig. 7(b) shows the numerically predicted stress field and extrusion profile for a damping factor of $k = 0.40$, which is close to that obtained from the simple shearing flow data. With the exception of the upstream heart shape, the stress contours appear qualitatively correct; however, with this k parameter the absolute values of the entry pressures and the die swell are too low.

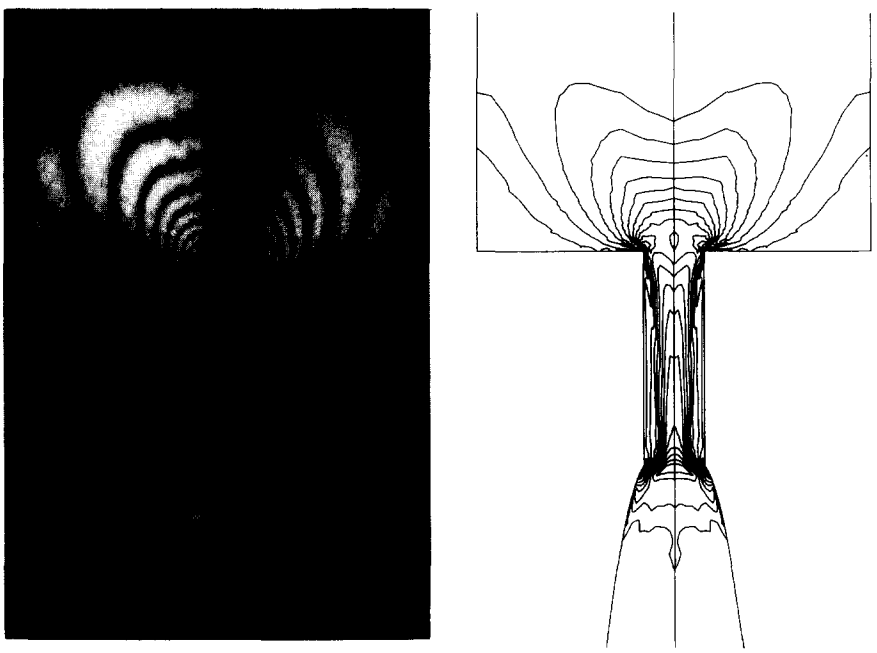

Fig. 4. Global stress field for HDPE Natene flowing into, within and out of the slit at 0.22 g s^{-1} and 180°C. (a) Experimental flow birefringence pattern, (b) numerical contours of principal stress difference obtained with Mesh 4 and $k = 0.35$.

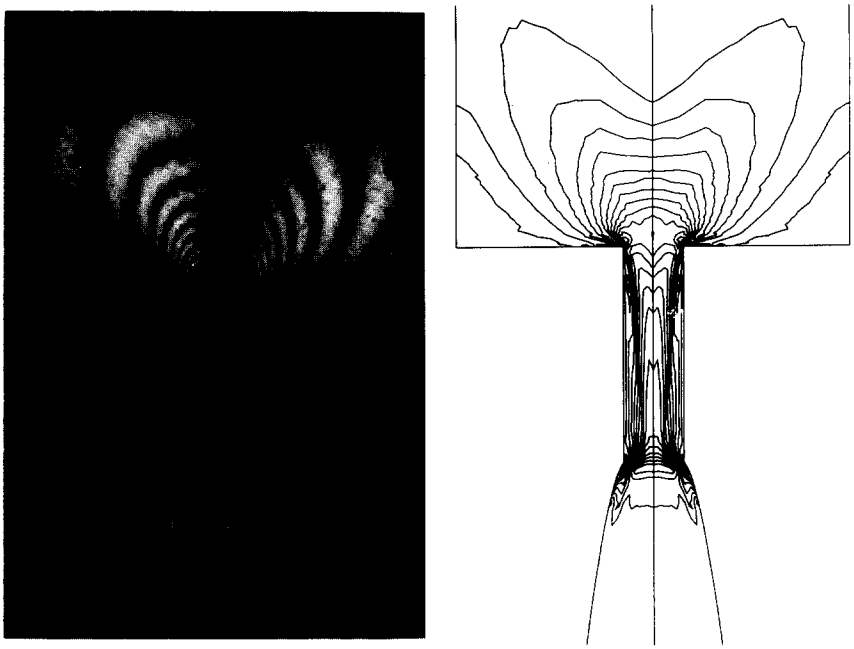

(a) (b)

Fig. 5. Global stress field for HDPE Natene flowing into, within and out of the slit at 0.32 g s^{-1} and 180°C. (a) Experimental flow birefringence pattern, (b) numerical contours of principal stress difference obtained with Mesh 4 and $k = 0.35$. The magnitudes of the experimental stress contours on the centre line correspond to data points given in Fig. 6.

In order to give a better match of both upstream profiles and die swell, the damping factor k was reduced and the profiles predicted for $k = 0.25$ are shown in Fig. 7(c). A reduction in k results in an increase in extensional strain hardening, and by reducing k from 0.40 to 0.25 both entry stress contours and die swell match experimental observation. A reduction in k also reduces the simple shear thinning response, and consequently the stress match near the walls of the slit is weakened by the change in k from 0.40 to 0.25. The simulation overpredicts the wall stress.

The quantitative behaviour of the centreline response is shown in Fig. 8. The crosses refer to the experimental data, and it can be seen that Polyflow with a simple shear value of $k = 0.40$ significantly underpredicts the stresses at all stages. An increase in the strain hardening brought about by a reduction in k to 0.25 greatly improves the match, and the experimental data lie between these results and the centreline simulation using our own laser velocimetry results and a k parameter of 0.20.

It is clear from these results that in the case of HDPE Rigidex, we are unable to obtain full self consistency using simple shear parameters alone. However, by suitable adjustment of k, both the correct entry flow and die swell behaviour can be predicted. In addition, the Natene and Rigidex simulations both show correct but different forms for the stress profiles in the throat region.

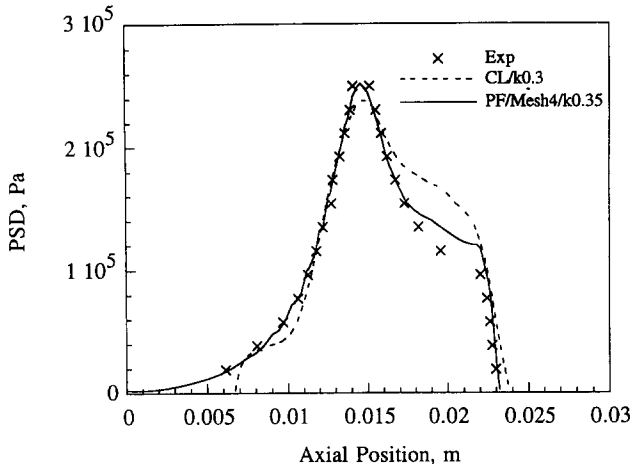

Fig. 6. Centreline stress profile (principal stress difference, PSD) as a function of axial position starting from the upstream entry for HDPE Natene flowing through the slit at 0.32 g s^{-1} and 180°C. ×, experimental data from flow birefringence; , numerical prediction using Polyflow with Mesh 4 and $k = 0.35$; ---, centreline prediction following flow kinematics with $k = 0.30$.

6.3. *The stress field and vortex recirculation for LDPE*

The flow behaviour of LDPE is shown in Figs. 9–11. The experimentally observed flow pattern for LDPE is profoundly different from that of HDPE, as shown in Fig. 9(a) which is the flow birefringence stress field. The entry flow region is dominated by the nearly stagnant recirculation vortices in the corner of the slit and the bulk flow appears to be constrained into the central region of the slit.

The simple shear damping factor for the LDPE was found to be $k = 0.16$. Computationally, we found that as k dropped below about 0.2 it became progressively more difficult to obtain a convergent solution. Fig. 9(b) shows the simulated principal stress contours obtained for LDPE with $k = 0.16$. Qualitatively, the stress contours show plausible agreement; however, quantitatively they underpredict the response.

This result is shown more clearly for the centreline behaviour given in Fig. 10. Again, the crosses correspond to the experimental flow birefringence data. The Polyflow simulation with $k = O.16$ significantly underpredicts the stresses. Using Polyflow, we were only able to obtain convergence down to a k factor of 0.086, and this result is also plotted in the Figure. Using this parameter, the match between simulation and experiment is improved but, in particular, the experimental peak stress is well above that of the simulation.

We were able to get a good match on the centreline using our own experimental laser velocimetry, velocity profile and a damping coefficient of 0.05, and this is also shown in Fig. 10. The result shows that the LDPE exhibits an extreme strain hardening response in extension. A k value of zero would correspond to a "Lodge elastic liquid" and in extensional flow the behaviour of the LDPE approaches this.

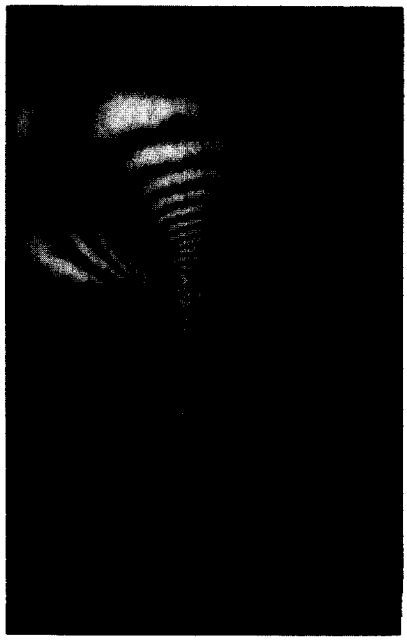

(a)

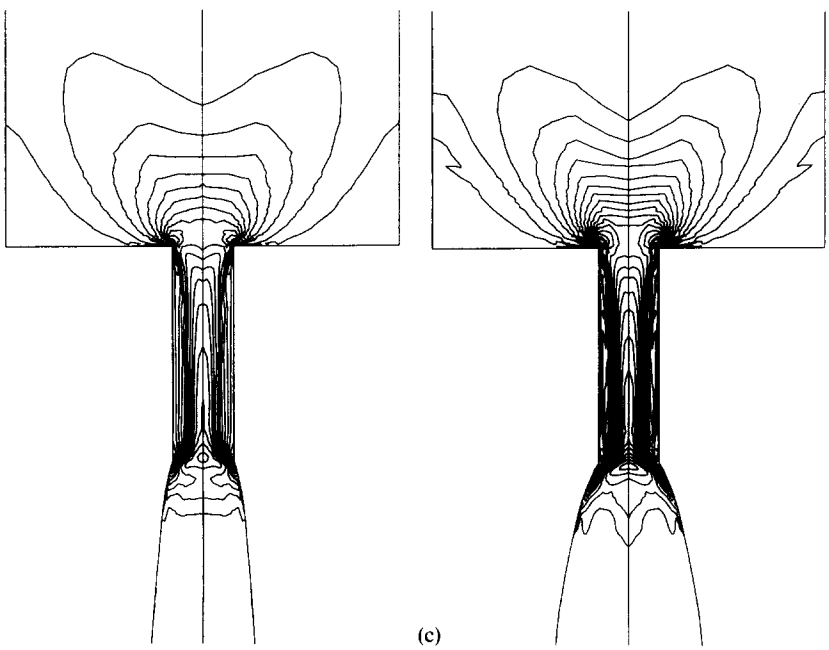

(b) (c)

Fig. 7. Global stress field for HDPE Rigidex flowing into, within and out of the slit at 0.22 g s^{-1} and 180°C. (a) Experimental flow birefringence pattern, (b) numerical contours of principal stress difference obtained with Mesh 4 and $k = 0.40$, (c) numerical contours of principal stress difference obtained with Mesh 4 and $k = 0.35$. The magnitudes of the experimental stress contours on the centreline correspond to data points given in Fig. 8.

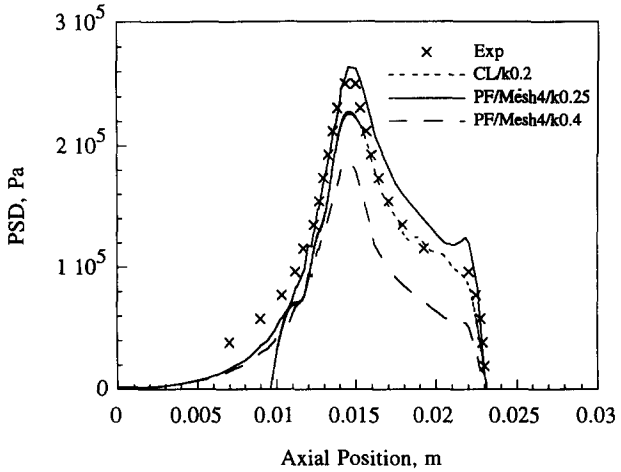

Fig. 8. Centreline stress profile (principal stress difference, PSD) as a function of axial position starting from the upstream entry for HDPE Rigidex flowing through the slit at 0.22 g s^{-1} and 180°C. ×, experimental data from flow birefringence; – – –, numerical prediction using Polyflow with Mesh 4 and $k = 0.40$; ——, prediction using Polyflow with Mesh 4 and $k = 0.25$; ---, centreline prediction following flow kinematics with $k = 0.20$.

As the damping factor is decreased, the numerical simulation successfully predicts the onset of recirculating vortices. This is shown in the streamline contours of Figs. 11(a) and 11(b) for damping coefficients of $k = 0.16$ and $k = 0.086$ respectively. The exact form of the recirculation does not match that observed in Fig. 9(a); however, we are reassured to see its emergence in the simulation as the level of extensional strain hardening increases. Our overall simulation results for LDPE have a similar trend to HDPE Rigidex. We are able to predict the correct overall form for the stress field, but have to use a different damping factor from that obtained from our simple shear rheological data.

6.4. *Velocity profiles*

Velocity is a further variable which needs to be matched between experimental data and simulation. In an entry flow, there are both radial and axial velocity components; however, we will only consider the axial velocity profile. In the present study, the experimental velocity profile is compared with the simulation and is also used as an input to compute the centreline stress profile using Eq. (6), as described in Ahmed and Mackley [1].

The comparison of velocity profile along the centreline between experiment and simulation has been made for the three materials tested and at different flow rates. A typical result is shown in Fig. 12 for HDPE Natene flowing into, within and out of the slit at a flow rate of 0.22 g s^{-1}. The centreline velocity profile is plotted as a function of axial position starting from the upstream entry. It is seen in Fig. 12 that whilst the overall forms of the profiles are similar, the absolute magnitudes for

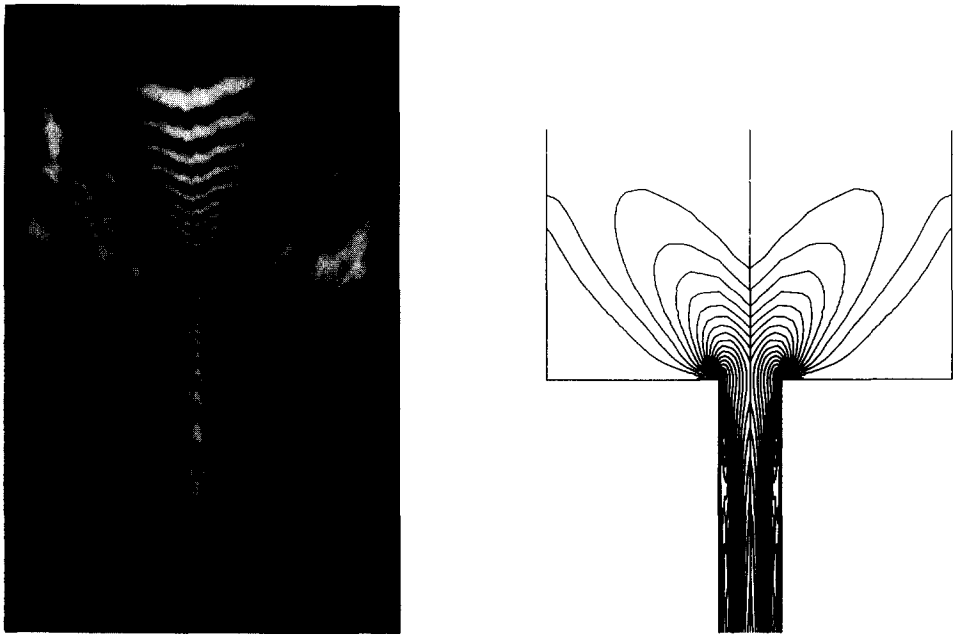

(a) (b)

Fig. 9. Global stress field for LDPE flowing into and through the slit at 0.32 g s^{-1} and 180°C. (a) Experimental flow birefringence pattern, (b) numerical contours of principal stress difference obtained with Mesh 2 and $k = 0.16$.

the velocities do not agree. The numerically predicted velocities are lower than the experimental data points. Concerning the profile shape, the velocity gradually builds up before the slit entrance corresponding to 0.015 m in Fig. 12, then shows a weak overshoot, and begins to decay at the slit exit at 0.023 m. It was found that a constant velocity shift factor exists between the experimental and numerical velocity profiles. As seen from Fig. 12, after the numerical velocity profile is multiplied by a factor of 1.2, the modified prediction data are able to fit the experimental data very well over the whole range including the downstream exit. Similar situations are also observed at other flow rates or for other materials, although the constant factor which indicates the deviation of the numerical velocity profile from the experimental measurement varies from one case to another. The results are summarized in Table 4(a). The largest factor of 1.64 was obtained for LDPE at a flow rate of 0.32 g s^{-1} while the factor for HDPE ranges between 1.64 and 1.2.

The shapes of our simulated "normalized" velocity profiles match the experimentally obtained velocity profiles within the precision of our experimental data. We have checked that nearly the same centreline stress profiles are obtained and predicted using either the experimentally measured flow kinematics or the Polyflow

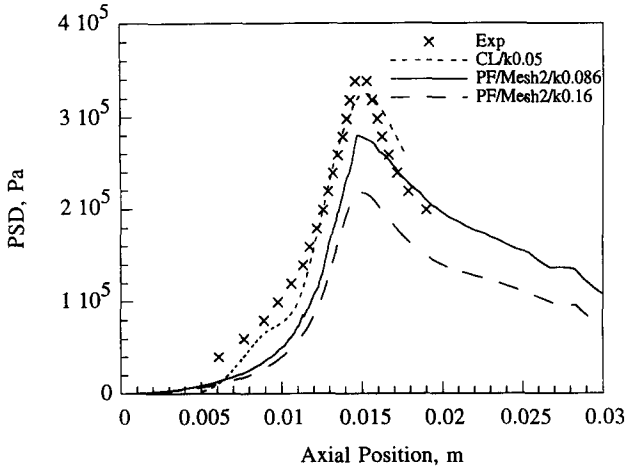

Fig. 10. Centreline stress profile (principal stress difference, PSD) as a function of axial position starting from the upstream entry for LDPE flowing through the slit at 0.32 g s^{-1} and 180°C. ×, experimental data from flow birefringence; – – –, numerical prediction using Polyflow with Mesh 2 and $k = 0.16$; , prediction using Polyflow with Mesh 2 and $k = 0.086$; ---, centreline prediction following flow kinematics with $k = 0.05$.

predicted velocity profile. The strain history measured by the Finger tensor, which is used in Eq. (6) to determine the centreline stress field, depends on the ratio of velocities at the present time t and past time t', rather than the absolute magnitude of the velocity. The stretching ratio does not change if the velocity is multiplied by a constant factor. We are fully confident in the relative velocity changes along the centreline, even if the absolute velocity is subject to error.

To explain the deviation of the numerical absolute velocities from the experimental results, various factors have been considered. Among these, the most plausible reason is the difference between the two-dimensional numerical simulation and the

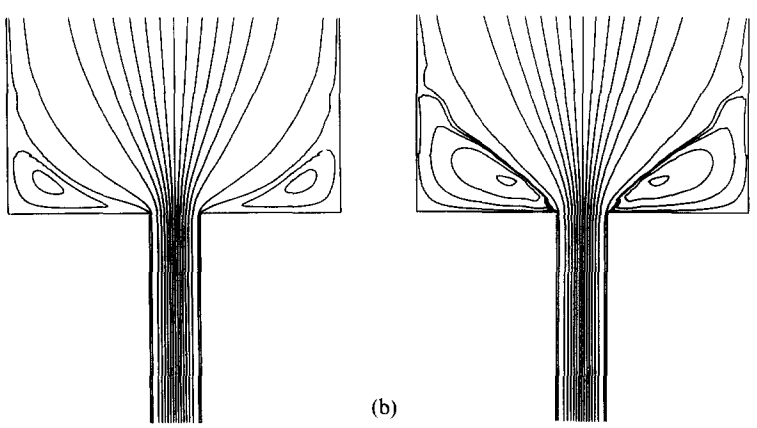

Fig. 11. Simulated streamline pattern for LDPE flowing into and through the slit at 0.32 g s^{-1} and 180°C with Mesh 2. (a) $k = 0.16$, (b) $k = 0.086$.

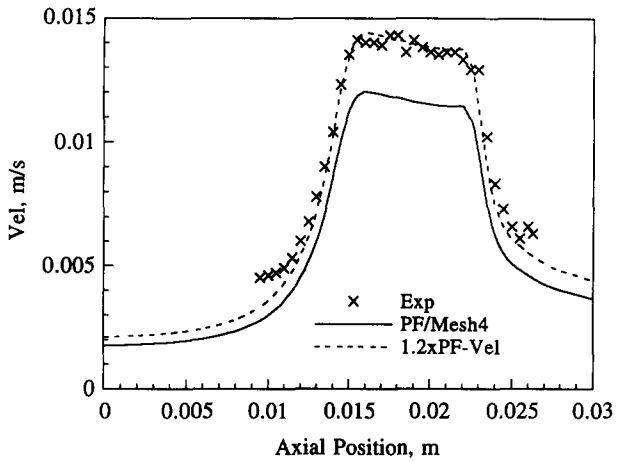

Fig. 12. Centreline velocity profile as a function of axial position starting from the upstream entry for HDPE Natene flowing into, within and out of the slit at 0.22 g s^{-1} and 180°C. ×, experimental data from laser velocimetry; numerical prediction using Polyflow (Mesh 4) with $k = 0.35$; ---, modified velocity profile obtained by multiplying the prediction by a factor of 1.22.

three-dimensional practical flow. In the experiment, the glass windows constrain the flow in the third direction (see Ahmed and Mackley [1]). To check the effect of a velocity component in the third dimension, we carried out a 3D simulation for a Newtonian fluid using Polyflow and the same experimental boundary conditions,

Table 4
(a) The comparison of experimental (3D) and numerical (2D) centreline velocities

Material	Flow rate (g s^{-1})	$V_{Exp,3D}/V_{Pflow,2D}$
Natene	0.22	1.22
	0.32	1.22
Rigidex	0.22	1.30
	0.44	1.40
LDPE	0.32	1.64

(b) The comparison of velocities between 3D and 2D Polyflow simulation and mathematical analysis for a Newtonian fluid

	$V_{3D,max}/V_{2D,max}$
Numerical simulation	
upstream of throat	1.40
downstream of throat	1.11
Mathematical analysis (see Appendix)	
upstream of throat	1.40
downstream of throat	1.11

i.e. upstream slit width 14.7 mm, downstream slit width 2.3 mm, slit depth 14.7 mm. The computed maximum velocity from the 3D simulation is larger than that from 2D simulation. The factor varies from 1.40 for the experimental slit upstream geometry to 1.11 for the experimental slit downstream geometry. In addition, the velocity profile can be obtained mathematically for a 3D infinitely long slit flow of a Newtonian fluid (see Appendix). The same result as that from the simulation is obtained. All these factors are also listed in Table 4(b). From the above discussion, we believe that the discrepancy in velocity between experiment and simulation can be ascribed to the fact that the experimental flow is 3D, while the simulation geometry is assumed as 2D.

Both viscoelastic and non-linear behaviour will also influence velocity profiles in 3D and 2D slit flow; however, at this stage the Polyflow numerical simulation cannot handle this additional complexity whilst at the same time using integral type constitutive equations.

6.5. Die swell

Die swell is a property of viscoelastic fluids which describes their ability to expand on extrusion from a constriction. We define the die swell ratio (B) as the ratio of the extrudate width at a set downstream position from the exit, to the width of the slit at the exit. The die swell ratio of an extrudate can be measured at different post extrusion positions. In this paper, we report the initial die swell ratio only, which is the swelling in the initial stages when polymer emerges out of the die and is measured at a set distance, 2 mm, downstream from the die exit.

The experimentally measured and numerically predicted die swell ratios for Natene and Rigidex are listed in Table 5. No die swell data were obtained for LDPE because of processing difficulties in forming a stable extrudate, as shown in Fig. 9(a).

For Natene, the Wagner equation and the simple shear damping coefficient, with the irreversible damping function, successfully give a realistic die swell prediction which is in good agreement with the measured die swell ratio. It is found that an

Table 5
Experimental data and numerical predictions for die swell ratio [a]

Material	Flow rate (g s^{-1})	Exp. die swell B	Polyflow pred. die swell		
			k factor	IR/R	B
Natene	0.22	1.46	0.35	IR	1.58
	0.22	1.46	0.35	R	1.64
	0.32	1.46	0.35	IR	1.57
Rigidex	0.22	1.62	0.25	IR	1.70
	0.22	1.62	0.40	IR	1.34

[a] Die swell ratios are taken 2 mm downstream from the slit exit. IR: irreversible damping function, R = reversible damping function and B = die swell ratio.

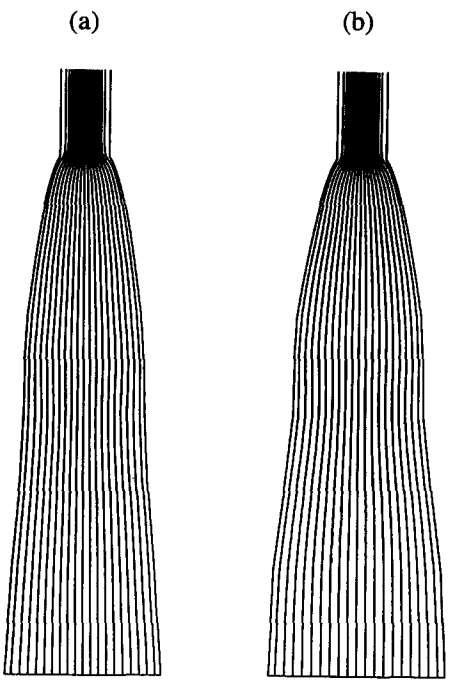

Fig. 13. Simulated streamline pattern and shape of the extrudate for HDPE Natene flowing out of the slit at 0.22 g s^{-1} and 180°C with Mesh 4 and $k = 0.35$: (a) using an irreversible damping function, (b) using a reversible damping function.

increase in the flow rate from 0.22 to 0.32 g s^{-1} does not influence the initial die swell result very much as observed in the measured data, although the die swell further downstream was influenced by flow rate. We have also looked at the effect of an irreversible or reversible damping function on the die swell prediction for Natene at a flow rate of 0.22 g s^{-1} with $k = 0.35$. Fig. 13(a) is the simulated streamline pattern and shape of the extrudate using the irreversibility assumption and Fig. 13(b) is the predicted streamline using the reversibility assumption. The choice of the reversibility assumption results in a larger die swell response. As seen from Table 5, the initial die swell ratio increases from 1.58 to 1.64 while the measured value is 1.46. The simulation results appear consistent with the results reported by Goublomme et al. [10], where the extrudate swell of a high-density polyethylene was also numerically predicted with the Wagner damping functions.

In the case of Rigidex, applying the simple shear parameters with $k = 0.40$, as used in Fig. 7, the simulation underpredicted the observed die swell. The initial die swell is found to be 1.34 compared to the experimental value of 1.62. It is found that the choice of k value also affects the die swell ratio. A smaller extensional damping function coefficient is required not only to describe the stretching behaviour in the entry flow upstream, but also to describe the elastic recovery in the exit flow downstream. A value of $k = 0.25$ was found to be able to provide a

Table 6
The comparison in damping function k value between simple shear and entry flow

	Natene	Rigidex	LDPE
k, simple shear	0.30	0.37	0.16
k, ext. flow	0.35	0.25	0.05
Eq. applicability	Good	Failure for strain hardening	Failure for strain hardening + vortex

realistic die swell prediction, giving a value 1.70 which is nearly the same as that measured.

The die swell simulation results show similar trends to the numerical simulation of the entry flow. Near self consistency between the measured and predicted die swell ratio is found for Natene, but in the case of Rigidex the numerical prediction can only be consistent with the experimental observation if an extensional flow damping parameter, rather than simple shear damping parameter, is chosen.

7. Discussion and conclusions

Self consistency in stress and die swell data between experiment and simulation was obtained for one polyethylene, Natene. In the case of Rigidex, it was found that numerical extensional flow behaviour in the entry flow and die swell in the exit flow could be matched with the experiment, provided that additional strain hardening was introduced to the Wagner damping function k by a reduction in the value of k from that obtained by simple shear measurements. In the case of LDPE, a significant difference was seen in the entry flow behaviour and the experimentally observed recirculation could be approximately simulated by a further increase in the entry flow strain hardening term.

In the 2D formulation, the Wagner constitutive equation used in this paper has a single damping function coefficient. Our results show that self consistency can be nearly achieved in shear and extension with one parameter k for Natene. However, in the cases of both Rigidex and LDPE, a single parameter k is inadequate and the constitutive equation fails for the extensional strain hardening behaviour of the materials. The comparison of k values between shear and extension for three materials is summarized in Table 6.

The results reported in this paper for HDPE Natene appear important, as they demonstrate that for this particular grade of polyethylene we have developed a method of characterization, a constitutive equation and a numerical simulation which have been combined to successfully predict an essentially engineering polymer melt processing flow. This offers encouragement that the basis for a scheme exists which can be used in a genuine engineering way to predict pressure drops, stress and velocity profiles, together with the very important commercial aspect of die swell. The scheme also indicates that polymer characterization using (g_i,λ_i)

linear viscoelastic data coupled with a non-linear damping function is a necessary but not necessarily sufficient condition to fully characterize a polymer melt.

The success of quantitatively predicting extensional centreline stresses and die swell is impressive; however, the realities of long computation times and the present restriction to 2D flow demonstrate that, even for this case, significant additional work still needs to be done.

The HDPE Rigidex and LDPE results present an additional difficulty. The simulation is able to predict entry flow behaviour and die swell, provided a damping parameter is chosen which gives greater strain hardening than would result from using the simple shear damping factor. The divergence in response appears to be sufficiently large to believe that experimental errors cannot explain the differences. As reported by Ahmed and Mackley [1], the experimental flow does have a third-dimension component and the simulation is restricted to fully two-dimensional flow. It is plausible that this may yield an explanation for the differences; however, we are of the opinion that the inconsistency lies within the formulation of the constitutive equation. In particular, the constitutive equation is written in a way that the stress does not depend on the past rotational component of the flow. It is plausible that polymer melt rheology is sensitive to rotation within the flow, and this effect would manifest itself in the simple shear flow behaviour that contains rotational components. If this hypothesis were correct the basic structure of the constitutive equation would have to be reformulated.

A satisfying aspect of the overall work was observing a match between experimental and numerical difficulties. HDPE Natene is an easily processed polymer and, provided a damping factor of the order $k = 0.3$ was used, a convergent solution to the simulation could be readily achieved. A value of $k = 0.3$ yields a near neutral strain softening or hardening in the entry flow. In contrast, LDPE is a difficult material to process and the recirculation vortices are evidence that the material is reluctant to flow into the slit. In addition, the rates described in this paper were close to the situation where the flow was becoming unsteady. Similar difficulties arose with the numerical simulation. As k was progressively decreased, the extensional strain hardening increased and numerical stability and convergence became more difficult. With $k = \mathrm{O}$ (i.e. Lodge like), convergence could not be obtained.

The above example shows a situation where numerical simulation is experiencing similar difficulties to experimental melt processing. In the future, this correlation should help in the design of particular polymer grades for different processing duties. Another notable feature is that the strategy described has successfully been able to predict differences in the die swell response of HDPE Natene and Rigidex, although the melt flow index and steady simple shear flow curves are very similar. From this it is apparent that the extensional flow behaviour of polymer melts is very important in understanding the full melt processing behaviour of polymers in general.

The observed differences in the magnitude of the experimentally determined velocities and the numerically predicted values can be explained by the fact that the numerical simulation is 2D, while the experiment geometry has a third dimension to

the velocity profiles. The shape of the experimental and numerical velocity profiles is in good agreement and the prediction of the stress field is essentially only dependent on the relative rather than absolute velocity changes. At present, there is little scope for performing full 3D numerical simulations or full 2D experimental extrusions.

Within the above limitations, we have been able to predict successfully both the entry and exit flow of three molten polyethylenes under study. It is clear that differences in extensional flow strain hardening can have a profound effect on processability, recirculation and die swell. These differences in extensional flow behaviour do not necessarily manifest themselves in any simple shearing flow characterization.

Acknowledgements

We wish to acknowledge the generous support of BP Chemicals in this work and, in particular, collaboration with Dr. G.C. Cappacio, Mr. C. Frye and Dr. P. Hope. We also thank Professor Crochet and his team for their assistance with the Polyflow software. The Appendix to this paper was kindly supplied by Dr. E.J. Hinch, DAMTP, University of Cambridge. We would also like to acknowledge further financial support from the NPL/DTI polymer processing program in the later stages of this project.

Appendix

Velocity profile for a 3D slit flow of a Newtonian fluid

Consider the unidirectional flow $u(y,z)$ of a Newtonian fluid of viscosity μ along an infinite channel in the x-direction, with a rectangular cross-section $-b \leqslant y \leqslant b$, $-c \leqslant z \leqslant c$. The momentum equation is then

$$0 = -\frac{\mathrm{d}p}{\mathrm{d}x}\mu\left(\frac{\partial^2 u}{\partial y^2} + \frac{\partial^2 u}{\partial z^2}\right),$$

where the y and z components indicate that the pressure is uniform across the cross-section. We solve this equation subject to the no-slip boundary conditions by superposing Fourier solutions, i.e. we pose

$$u(y,z) = \sum_{mn} A_{mn} \sin\frac{m\pi(y+b)}{2b} \sin\frac{n\pi(z+c)}{2c}.$$

This satisfies the no-slip boundary conditions on $y = -b$ and b on $z = -c$ and c. Substituting the sum into the momentum equation, we obtain

$$0 = -\frac{\mathrm{d}p}{\mathrm{d}x} - \mu\sum_{mn} A_{mn}\frac{\pi^2}{4}\left(\frac{m^2}{b^2} + \frac{n^2}{c^2}\right)\sin\frac{m\pi(y+b)}{2b} \sin\frac{n\pi(z+c)}{2c}.$$

Multiplying by $\sin[k\pi(y+b)/2b]\sin[l\pi(z+c)/2c]$ where k and l are integers and integrating over the channel, we obtain

$$0 = -\frac{\mathrm{d}p}{\mathrm{d}x}\frac{16bc}{\pi^2 kl} - \mu A_{kl}\frac{\pi^2 bc}{4}\left(\frac{k^2}{b^2}+\frac{l^2}{c^2}\right),$$

if k and l are both odd, and otherwise $A_{kl}=0$.

We can now relate the maximum velocity and the average velocity to the pressure gradient:

$$U_{\max} = u(0,0) = \sum_{mn} A_{mn}\sin\frac{m\pi}{2}\sin\frac{n\pi}{2} = -\frac{\mathrm{d}p}{\mathrm{d}x}\frac{b^2}{\mu}f(b/c)$$

where

$$f(b/c) = \frac{64}{\pi^4}\sum_{mn\,\mathrm{odd}}\frac{c^2(-1)^{(m+n)/2+1}}{mn(m^2c^2+n^2b^2)},$$

$$U_{\mathrm{av}} = \frac{1}{24bc}\int_{-b}^{b}\int_{-c}^{c} u(y,z)\,\mathrm{d}y\,\mathrm{d}z = \sum_{mn}\frac{4}{\pi^2 mn}A_{mn} = -\frac{\mathrm{d}p}{\mathrm{d}x}\frac{b^2}{\mu}g(b/c)$$

where

$$g(b/c) = \frac{256}{\pi^6}\sum_{mn\,\mathrm{odd}}\frac{c^2}{m^2n^2(m^2c^2+n^2b^2)}.$$

In the case of a very wide channel $c \gg b$, we recover the 2D result with

$$f(0) = 1/2 \quad \text{and} \quad g(0) = 1/3$$

In the case of the experimental conditions $b/c = 2.3/14.7 = 0.1565$ and $b/c = 14.7/14.7 = 1.0$, we find numerically

$$f(0.1565) = 0.50 \quad \text{and} \quad g(0.1565) = 0.30$$

$$f(1.0) = 0.294 \quad \text{and} \quad g(1.0) = 0.14$$

Hence, making a comparison at constant volume flux, i.e. the same average velocity, the ratios of the maximum velocity in the 3D experimental conditions to that in a very wide 2D channel are

$$\frac{f(0.1565)}{g(0.1565)}\Big/\frac{f(0)}{g(0)} = 1.11$$

$$\frac{f(1.0)}{g(1.0)}\Big/\frac{f(0)}{g(0)} = 1.40$$

References

[1] R. Ahmed and M.R. Mackley, Experimental centreline planar extension of polyethylene melt flowing into a slit die, J. Non-Newtonian Fluid Mech., 56 (1995) 127–149.

[2] S.T.E. Aldhouse, M.R. Mackley and I.P.T. Moore, Experimental and linear viscoelastic stress distribution measurements of high density polyethylene flowing into and within a slit, J. Non-Newtonian Fluid Mech., 21 (1986) 359–376.
[3] M.R. Mackley and I.P.T. Moore, Experimental velocity distribution measurements of high density polyethylene flowing into and within a slit, J. Non-Newtonian Fluid Mech., 21 (1986) 337–358.
[4] M.J. Crochet and K. Walters, Computational rheology: a new science, Endeavour, New Series, 17(2) (1993) 64–77.
[5] S. Dupont and M.J. Crochet, The vortex growth of a K-BKZ fluid in an abrupt contraction, J. Non-Newtonian Fluid Mech., 29 (1988) 81–91.
[6] M. van Gurp, C.J. Breukink, R.J.W.M. Sniekers and P.P Tas, Rheological characterization of low density polyethylene in planar extension using rheo-optics, SPIE, Laser Anemometry Advances and Applications, 2052 (1993) 297–304.
[7] K. Feigl and H.C. Ottinger, The flow of a LDPE melt through an axisymmetric contraction: a numerical study and comparison to experimental results, J. Rheol., 38 (1994) 847–874.
[8] H.J. Park, D.G. Kiriakidis, E. Mitsoulis and K.-J. Lee, Birefringence studies in die flows of an HDPE melt, J. Rheol., 36 (1992) 1563–1583.
[9] D.G. Kiriakidis, H.J. Park, E. Mitsoulis, B. Vergnes and J.-F. Agassant, A study of stress distribution in contraction flows of an LLDPE melt, J. Non-Newtonian Fluid Mech., 47 (1993) 339–356.
[10] A. Goublomme, B. Draily and M.J. Crochet, Numerical prediction of extrudate swell of a high-density polyethylene, J. Non-Newtonian Fluid Mech., 44 (1992) 171–195.
[11] A. Goublomme and M.J. Crochet, Numerical prediction of extrudate swell of a high-density polyethylene: further results, J. Non-Newtonian Fluid Mech., 47 (1993) 281–287.
[12] R.J. Koopmans, Extrudate swell of high density polyethylene, Polym. Eng. Sci., 32 (1992) 1741–1764.
[13] Polyflow Manual, Theoretical Background, Polyflow s.a., Belgium, 1990.
[14] Polyflow Manual, User's Manual, Polyflow s.a., Belgium, 1992.
[15] M.H. Wagner, Analysis of time-dependent nonlinear stress-growth data for shear and elongational flow of a low density branched polyethylene melt, Rheol. Acta., 15 (1976) 136–142.
[16] M.H. Wagner, Zur Netzwerktheorie von Polymer-Schmelzen, Rheol. Acta, 18 (1979) 33–50.
[17] J.M. Dealy and K.F. Wissbrun, Melt Rheology and its Role in Plastics Processing, Van Nostrand Reinhold, New York, 1990.
[18] H.M. Laun, Description of the non-linear shear behaviour of a low density polyethylene melt by means of an experimentally determined strain dependent memory function, Rheol. Acta, 17 (1978) 1–15.
[19] M.R. Mackley, R.T.J. Marshall, J.B.A.F. Smeulders and F.D. Zhao, The rheological characterization of polymeric and colloidal fluids, Chem. Eng. Sci., 49 (1994) 2551–2565.
[20] R.F. Liang and M.R. Mackley, Rheological characterization of the time and strain dependence for polyisobutylene solutions, J. Non-Newtonian Fluid Mech., 52 (1994) 387–405.
[21] M.H. Wagner and S.E. Stephenson, The irreversibility assumption of network disentanglement in flowing polymer melts and its effects on elastic recoil predictions, J. Rheol., 23 (1979) 489–504.